# Scaling of the velocity field induced by a bubble rising rectilinearly through liquid under variation of the gas-liquid density ratio

## M. Wörner

*Forschungszentrum Karlsruhe GmbH, Institut für Reaktorsicherheit, Postfach 3640, 76021 Karlsruhe Germany, E-mail: woerner@irs.fzk.de*

**Abstract**

The present numerical study investigates the influence of the gas-liquid density ratio on bubble shape and bubble Reynolds number ($Re_B$) by 3D volume-of-fluid computations. For fixed values of the Eötvös number ($Eö_B = 3.06$) and the Morton number ($M = 3.09 \cdot 10^{-6}$) and the unity viscosity ratio four cases are considered, where the liquid density is 2, 5, 10, and 50 times the gas density. All the simulations result in an oblate ellipsoidal bubble that rises steadily on a rectilinear path. Due to the added mass force the density ratio has a notable influence in the initial stage when the bubble accelerates from rest to its terminal velocity. Once the bubble has reached its terminal velocity, the dependence of the bubble Reynolds number and the ellipse aspect ratio on the density ratio are very weak. The computed value for $Re_B$ agrees well with a relation derived from two-fluid wave theory that expresses $Re_B$ as function of $Eö_B$ and $M$. The local profile of liquid and gas velocity along a vertical line through the bubbles centroid is found to be independent of the density ratio, when scaled by the bubble rise velocity.

## INTRODUCTION

The contacting of liquid and gas bubbles is an efficient process for achieving high rates of heat and/or mass transfer. As a consequence, the buoyancy-driven motion of bubbles or drops is of considerable practical importance in many industrial branches, e.g. in chemical and nuclear engineering. The buoyancy-driven motion of fluid particles is, however, also of great scientific interest as the complex interaction of buoyancy forces, capillary forces, viscous forces and inertia forces can result in various types of bubble motion (rectilinear, zig-zag, spiral, irregular, ...) and bubble shapes (spherical, ellipsoidal, "wobbling", cap-type, ...).

Despite the enormous amount of research that has been devoted to the buoyancy-driven motion of bubbles and drops in the past, there are still some aspects that are not fully clarified. For example, the influence of the disperse-to-continuous phase density ratio as one of the fundamental similarity parameters determining the shape and rise of fluid particles has attracted rather little attention up to now. Associated with the development of advanced methods for direct numerical simulation (DNS) of interfacial flows and the availability of more and more powerful computers there is, however, an increased interest to quantify the influence of the density ratio. This is because in two-phase flow a DNS is often not performed for a density ratio of about 1/1000, as it is typical for air bubbles in water. Instead, in order to avoid numerical problems and to minimize the computational costs, a density ratio larger than 1/100 is often chosen. Ye et al. [20], for example note that for a large density ratio the disparity of the fluid property across the interface makes the computation stiff and often leads to numerical instability. Bunner & Tryggvason [2] observe that their multi-grid solver fails to converge in the solution of the pressure Poisson equation if the density ratio is very small.

They state that a SOR solver is more robust, but its use is impractical because it increases the computational time required to achieve the same accuracy by one to two orders of magnitude. Another drawback of density ratios substantially different from unity is the difference in diffusive time scale of both phases. Wörner [18] reports that the maximum time step size allowed for numerical stability of an explicit time integration scheme decreases almost linear as the density ratio decreases. For all these reasons it appears favorable to perform simulations with a density ratio of order 1/10 or 1/100 instead of 1/1000. This, however, raises the important question to what extent results obtained from such simulations can be transferred to gas-liquid systems of higher density ratio.

Before we address this question by screening the relevant literature, we first recall some results of similitude analysis to facilitate the understanding of what will follow. For a fluid particle rising with its terminal velocity through an infinite liquid the physical quantities of influence are included in the following equation [7]:

$$F^* \left( g^*, \rho_c^*, \mu_c^*, \sigma^*, \rho_d^*, \mu_d^*, d_V^*, U_T^* \right) = 0 \,. \tag{1}$$

Here $\rho^*$ denotes the density, $\mu^*$ the dynamic viscosity, $g^*$ the acceleration of gravity, $\sigma^*$ is the coefficient of surface tension, $d_V^*$ the volume-equivalent diameter of the fluid particle and $U_T^*$ is its terminal rise velocity. The indices $d$ and $c$ denote the dispersed and continuous phase, respectively, and $^*$ is used to indicate a dimensional quantity. Similitude analysis shows that the above equation may be rewritten in terms of five independent dimensionless groups [4, 7]. For example, the bubble Reynolds number $Re_B \equiv \rho_l^* d_V^* U_T^* / \mu_l^*$, which may be interpreted as non-dimensional bubble rise velocity, is a function of Morton number $M \equiv (\rho_l^* - \rho_g^*) g^* \mu_l^{*4} / (\rho_l^{*2} \sigma^{*3})$, of bubble Eötvös number $Eö_B \equiv (\rho_l^* - \rho_g^*) g^* d_V^{*2} / \sigma^*$, and of the ratios of disperse-to-continuous density $\Gamma_\rho = \rho_d^* / \rho_c^*$ and viscosity $\Gamma_\mu = \mu_d^* / \mu_c^*$:

$$Re_B = f\left(M, Eö_B, \Gamma_\rho, \Gamma_\mu\right) \,. \tag{2}$$

Note that in Eq. (2) any of the non-dimensional groups $Re_B$, $M$, $Eö_B$ can be replaced by the Weber number in virtue of the identity $We_B \equiv \rho_l^* d_V^* U_T^{*2} / \sigma^* = Re_B^2 \sqrt{M / Eö_B}$. Here, we prefer to use the non-dimensional groups according to Eq. (2) because in this case for all five groups there is only one group ($Re_B$) that incorporates the rise velocity $U_T^*$ and only one group ($Eö_B$) that incorporates the equivalent diameter $d_V^*$.

Experimental studies on the influence of the density ratio as a similarity parameter are rare. The reason is that the density ratio is no parameter which can be easily varied in an experiment, while at the same time all the other parameters are kept constant. In the course of an experimental series, usually one specific continuous phase and various dispersed phases are used, or vice versa. In general, by this approach together with the density ratio also the viscosity ratio and the Morton number are varied. This procedure is therefore unsuited to reveal the specific functional dependence of $Re_B$ on $\Gamma_\rho$ expressed by Eq. (2). Nevertheless, Grace [7] notes that for bubbles rising in liquids $\Gamma_\rho$ and $\Gamma_\mu$ tend to be very small so that the density and viscosity of the dispersed phase become unimportant causing $Re_B = f(M, Eö_B)$.

The specific influence of the density ratio can be investigated more easily by means of numerical simulation. Dandy & Leal [6] study the steady axisymmetric motion and deformation of a fluid particle in a streaming flow by a finite-difference scheme using the stream function-vorticity formulation of the Navier-Stokes equation and a boundary-fitted orthogonal coordinate system. The authors consider both the case of a bubble and a drop. For the bubble the viscosity ratio is 1 and the values of the Reynolds and Weber number are fixed to $Re_B = 100$, $We_B = 4$, while two values of the density ratio are considered: $\Gamma_\rho = 0.1$ and $0.01$.

For the drop they use $Re_B = 60$, $We_B = 4$, $\Gamma_\mu = 100$ and the values of the density ratio are $\Gamma_\rho =$ 10, 100, and 1000. The authors find that the variation of the density ratio produces only a slight change in shape and flow field. They state that "the only surprise is that the effect of variation of the density ratio is so weak". Recently, Ye et al. [20] developed a combined Eulerian-Lagrangian method where the Navier-Stokes equation is solved on a fixed grid and the interface is explicitly defined by geometric curves in the computational domain. They compute the rise of an axisymmetric bubble for the same constant parameters as Dandy & Leal (i.e. $Re_B = 100$, $We_B = 4$, $\Gamma_\mu = 1$), but consider values of the density that span three orders of magnitude: $\Gamma_\rho = 0.1$, 0.01, 0.001. They confirm that the differences are small, but observe that for the higher values of $\Gamma_\rho$ the bubble is slightly less deformed.

Oka & Ishii [11] performed 3D simulations of a single bubble rising through a viscous liquid in a square duct by a level-set method. They introduce the reduced Morton number $M^\dagger = M/(1-\Gamma_\rho)$ and reduced Eötvös number $E\ddot{o}^\dagger = E\ddot{o}/(1-\Gamma_\rho)$ and perform simulations for fixed values $M^\dagger = 3.125\cdot10^{-3}$, $E\ddot{o}^\dagger = 20$ for three different values of the density ratio $\Gamma_\rho =$ 0.02, 0.01, 0.001. They find that the effect of variation of the density ratio on the cap-type bubble shape and the flow field is extremely weak when $\Gamma_\rho$ is smaller than 0.02. Additionally, they perform a run with $\Gamma_\rho = 0.1$ and $M^\dagger = 3.125\cdot10^{-3}/(1-0.1) = 3.472\cdot10^{-3}$ and $E\ddot{o}^\dagger = 20/(1-0.1) = 22.22$. By this choice of $M^\dagger$ and $E\ddot{o}^\dagger$ they take into account the effect of the change of the density difference $\Delta\rho^*$ that results from variation of the density ratio and thus ensure that in all four runs the values of $M$ and $E\ddot{o}_B$ are (almost) identical. Oka & Ishii [11] find that in the run with $\Gamma_\rho = 0.1$ the rise velocity is about 5.5% less than in the run with $\Gamma_\rho = 0.001$.

Bunner & Tryggvason [2] perform simulations of 3D bubbly flow for $E\ddot{o}_B = 1$ and $M = 1.23\cdot10^{-6}$ using $\Gamma_\rho = 0.02$. They justify this choice by the observation that in 2D tests using much smaller density ratios the effect of the density ratio and of the inertia of the fluid inside the bubble is small for these values [16]. Though we note that there exist some further numerical studies on the influence of the density ratio, e.g. those by Chen et al. [3] and Juncu [8], we do not review these here because there together with the density ratio also the Eötvös number and Morton number are varied.

The present investigation is motivated by recent results of Sabisch [12] (see also [13]) who performed 3D simulations of a single bubble rising through an initially quiescent liquid within a vertical channel by the volume-of-fluid (VOF) method. For the density ratio he used $\Gamma_\rho = 0.5$ and for the viscosity ratio $\Gamma_\mu = 1$. He considered four different combinations of ($M$, $E\ddot{o}_B$) which were chosen so that from the diagram of Clift, Grace, and Weber (CGW) [5, p. 27] in which $Re_B$ is displayed as function of ($M$, $E\ddot{o}_B$) a spherical, ellipsoidal, oblate spherical cap, and a wobbling bubble shape should be expected. Despite the density ratio 0.5, the Reynolds number, shape, rising path, and wake type of the bubble agreed qualitatively very well with the diagram of CGW for all four different combinations of ($M$, $E\ddot{o}_B$). Due to the qualitative agreement of the bubble shape and Reynolds number computed for $\Gamma_\rho = 0.5$ with the diagram of CGW (deduced from experiments with $\Gamma_\rho \approx 0.001$) for fixed values of ($M$, $E\ddot{o}_B$) one may conjecture that the dependence of the bubble Reynolds number on the density ratio is weak in general, not only for $\Gamma_\rho < 0.02$. In this paper results obtained by the same code as in [12, 13] are presented for fixed parameters of the ellipsoidal bubble case, i.e. for $M=3.09\cdot10^{-6}$, $E\ddot{o}_B=3.06$, $\Gamma_\mu = 1$, but for different values of the density ratio: $\Gamma_\rho = 0.5$, 0.2, 0.1, 0.02. It will be shown (see also [18]) that the density ratio is of relevance for the initial phase when the bubble accelerates from rest to its terminal velocity. Once the bubble has attained its steady rise velocity, both the bubble shape and bubble Reynolds number are not affected by the density ratio. In broadening the analysis of [18], where we considered only the bubble rise velocity as an integral quantity of the system, we now also investigate the scaling of the local velocity field, both in the gas and liquid phase.

# SIMULATION METHOD

In this chapter we shortly present the governing equations and the numerical method, followed by the specification of the computational configuration as well as the parameters of the simulations.

## Governing equations

To obtain non-dimensional equations we adopt the following normalization

$$\vec{x} = \begin{pmatrix} x \\ y \\ z \end{pmatrix} = \frac{\vec{x}^*}{L_{ref}^*}, \ \vec{u} = \frac{\vec{u}^*}{U_{ref}^*}, \ t = \frac{t^* U_{ref}^*}{L_{ref}^*}, \ \rho = \frac{\rho^*}{\rho_c^*}, \ \mu = \frac{\mu^*}{\mu_c^*}, \ P = \frac{p^* - \rho_c^* \vec{g}^* \cdot \vec{x}^*}{\rho_c^* U_{ref}^{*2}},$$

Here, $L_{ref}^*$ and $U_{ref}^*$ are a reference length and reference velocity, respectively. Note that in the non-dimensional pressure we account for hydrostatic effects so that the buoyancy force appears in the momentum equation as a source term instead of the gravity force. In non-dimensional form this results in the appearance of the Eötvös number instead of the Froude number. In the context of Eq. (2) this is of certain advantage here. With the above normalization, the non-dimensional volume-averaged continuity equation is given by

$$\nabla \cdot \vec{u}_m = 0, \tag{3}$$

and the non-dimensional volume-averaged Navier-Stokes equation by

$$\frac{\partial \rho_m \vec{u}_m}{\partial t} + \nabla \cdot \rho_m \vec{u}_m \vec{u}_m = -\nabla P + \frac{1}{Re_{ref}} \nabla \cdot \mu_m \left( \nabla \vec{u}_m + (\nabla \vec{u}_m)^{\mathrm{T}} \right) - (1-f) \frac{E\ddot{o}_{ref}}{We_{ref}} \frac{\vec{g}^*}{g^*} + \frac{\kappa \vec{n} a_{int}}{We_{ref}}. \tag{4}$$

In the latter two equations $\vec{u}_m$ is the non-dimensional center of mass velocity

$$\vec{u}_m \equiv \frac{1}{U_{ref}^*} \frac{f \rho_c^* \vec{u}_c^* + (1-f) \rho_d^* \vec{u}_d^*}{f \rho_c^* + (1-f) \rho_d^*},$$

where $f$ is the volumetric fraction of the continuous (liquid) phase within the averaging volume $V$, and $\rho_m$ and $\mu_m$ are the non-dimensional mixture density and viscosity, respectively,

$$\rho_m \equiv \frac{f \rho_c^* + (1-f) \rho_d^*}{\rho_c^*} = f + (1-f) \Gamma_\rho, \qquad \mu_m \equiv \frac{f \mu_c^* + (1-f) \mu_d^*}{\mu_c^*} = f + (1-f) \Gamma_\mu.$$

The last term in Eq. (4) expresses the effect of surface tension. There, $\kappa$ is the interface curvature, $\vec{n}$ is the unit normal vector to the interface, and $a_{int}$ is the interfacial area concentration within the mesh volume. The definitions of the reference Reynolds number ($Re_{ref}$), reference Eötvös number ($E\ddot{o}_{ref}$), and reference Weber number ($We_{ref}$) appearing in Eq. (4) are equivalent to those of $Re_B$, $E\ddot{o}_B$, and $We_B$ given above, but $U_T^*$ is replaced by $U_{ref}^*$ and $d_V^*$ is replaced by $L_{ref}^*$. The set of equations is completed by the transport equation for the liquid volumetric fraction

$$\frac{\partial f}{\partial t} + \nabla \cdot (f \vec{u}_m) = 0. \tag{5}$$

The derivation of the above set of volume-averaged volume-of-fluid equations is given in [19]. The form of equations (3) and (4) already implies that within volume $V$ both phases share the same pressure and the same velocity. The latter assumption corresponds to a locally homogeneous model. Equations (3) and (4) do not account for contamination of the interface by surfactants. The results to be presented thus correspond to a "pure" system.

## Numerical method

For the solution of the $f$-equation (5) by the VOF method we have developed a new algorithm called EPIRA (Exact Plane Interface Reconstruction Algorithm) [12, 13], which

belongs to the class of PLIC (Piecewise Linear Interface Calculation) methods. EPIRA reconstructs a plane 3D interface correctly, regardless of its orientation. The EPIRA algorithm has been implemented in our in-house computer code TURBIT-VOF [12], which solves the non-dimensional continuity and Navier-Stokes equations (3) and (4) together with the $f$-equation (5). TURBIT-VOF is designed to simulate flows in plane channels. It employs a staggered grid, uniform in the $x$- and $y$-directions (parallel to the walls), but possibly non-uniform in $z$-direction (normal to the walls). A second order central difference scheme is used to discretize the diffusive and non-linear convective terms in the Navier-Stokes equation. For discretization of the surface tension term we refer to [13]. The solution algorithm in TURBIT-VOF is based on a projection method. Starting from the results at time level $n$, a predictor step is performed by an explicit third order Runge-Kutta time integration scheme where the pressure term is neglected. This yields an intermediate non-solenoidal velocity field. In the corrector step this intermediate velocity field is projected to the divergence free velocity field $\vec{u}_m^{n+1}$ at the new time level $n+1$. As the pressure is treated implicitly, the corrector step requires the solution of the pressure Poisson equation. This is done by a conjugate gradient method. For further details of the numerical method as well as for verification of the code by several benchmark problems we refer to [12, 13].

## Computational grid, boundary conditions, and initial conditions

Figure 1 shows the coordinate system and a sketch of the computational domain. The $x$-, $y$- and $z$-axes were assigned in vertical direction, in transverse direction, and in wall-normal direction, respectively. The gravity vector points in negative $x$-direction. In $x$- and $y$-direction we have periodic boundary conditions; at $z = 0$ and $z = 1$ we have rigid walls and no-slip boundary conditions. The size of the computational domain is $L_x^* \times L_y^* \times L_z^* = 2 L_{ref}^* \times L_{ref}^* \times L_{ref}^*$. This domain is discretized by $128 \times 64 \times 64$ uniform mesh cells resulting in $\Delta x = \Delta y = \Delta z = 0.015625$. At time $t = 0$ a spherical bubble of diameter $d_V^* = L_{ref}^*/4$ is positioned in the domain with its center located at (0.5, 0.5, 0.5). Thus, in terms of the bubble diameter the size of the computational box is $8 \times 4 \times 4$. The diameter of the bubble is resolved by 16 mesh cells. The overall void fraction is about 0.4 %. Both, liquid and gas are initially at rest.
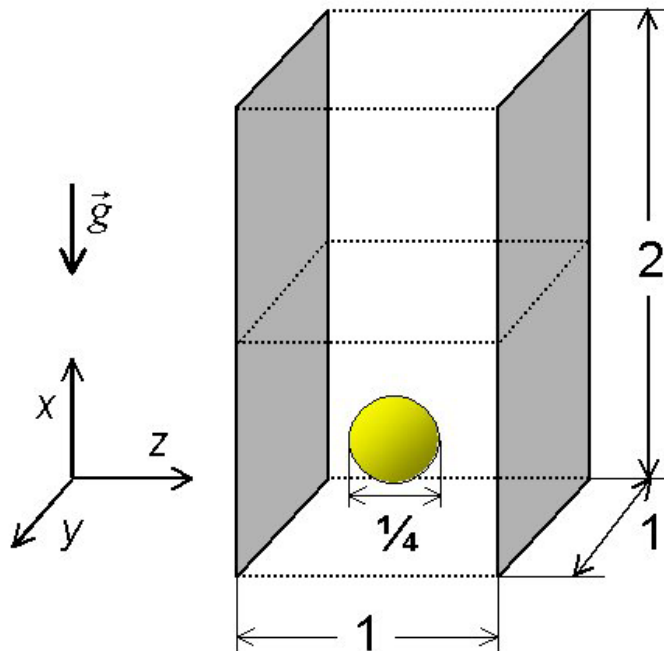


Fig. 1: Sketch of coordinate system and computational domain.

Due to the lateral walls and because we use periodic boundary conditions in $x$- and $y$-direction, the physical quantities of influence given in Eq. (1) are no longer complete and do not fully characterize the problem. While the only length scale in Eq. (1) is the bubble diameter, we have now three additional length scales due to our finite computational domain, namely $L_x^*, L_y^*, L_z^*$. Thus, the non-dimensional groups as given by Eq. (2), which only apply to a single bubble rising in an infinite fluid, should be extended by $d_V^*/L_x^*, d_V^*/L_y^*, d_V^*/L_z^*$. One can, however, argue that with the hydraulic diameter $d_h^* = 2L_{ref}^*$ the ratio $d_V^*/d_h^*$ takes a value of 0.125 and thus the wall influence is already small [5, p. 233]. Furthermore, we will restrict our analysis to the stage when the interaction with the "leading" and "trailing" bubble is small and thus stop the simulations when the bubble has risen a vertical distance of about half of the height of the computational domain. The results should then be comparable to that of a single bubble and altogether the influence of $d_V^*/L_x^*, d_V^*/L_y^*, d_V^*/L_z^*$ should be small.

## Parameters of the simulations

To set up the simulations we must specify the reference quantities $Re_{ref}$, $Eö_{ref}$, and $We_{ref}$ in the Navier-Stokes equation (4). We proceed as follows. We consider fixed values for the Morton number ($M = 3.09 \cdot 10^{-6}$), the bubble Eötvös number ($Eö_B = 3.06$), and the viscosity ratio ($\Gamma_\mu = 1$) and set $L_{ref}^* = 4\,\mathrm{m}$, $U_{ref}^* = 1\,\mathrm{ms}^{-1}$, $g^* = 9.81\ \mathrm{ms}^{-2}$. The only parameter we vary is the density ratio $\Gamma_\rho$. We then can successively compute

$$Eö_{ref} = \left(\frac{L_{ref}^*}{d_V^*}\right)^2 Eö_B, \quad We_{ref} = \frac{Eö_{ref}}{1-\Gamma_\rho}\frac{U_{ref}^{*\,2}}{g^* L_{ref}^*}, \quad Re_{ref} = \left(\frac{Eö_{ref}We_{ref}^2}{M}\right)^{0.25}.$$

In Table 1 we give the input values $Re_{ref}$, $Eö_{ref}$, and $We_{ref}$ for the different density ratios considered in the present study. Additionally, we give the values of $We_{ref}$ and $Re_{ref}$ for the asymptotic case $\Gamma_\rho \to 0$. It is important to note that in our simulations we do not specify any explicit values for the fluid properties $\rho_l^*, \mu_l^*, \sigma^*, \rho_g^*, \mu_g^*$. From similitude analysis, however, we know that the computed results are valid for any combination of fluid properties that results in the values of $M$, $Eö_B$, $\Gamma_\rho$, and $\Gamma_\mu$ used in the respective simulation run.

Table 1: Parameters of the simulations for different values of the density ratio ($\Delta t$ is the time step and $N_t$ is the number of time steps computed).

| Run | $\Gamma_\rho$ | $1/\Gamma_\rho$ | $Eö_{ref}$ | $We_{ref}$ | $Re_{ref}$ | $\Delta t$ | $N_t$ |
|-----|-----|-----|-----|-----|-----|-----|-----|
| M2 | 0.5 | 2 | 49.05 | 2.5 | 100.0 | 0.0005 | 1,100 |
| M5 | 0.2 | 5 | 49.05 | 1.5625 | 78.898685 | 0.0003 | 1,800 |
| M10 | 0.1 | 10 | 49.05 | 1.3888 | 74.386394 | 0.00015 | 3,200 |
| M50 | 0.02 | 50 | 49.05 | 1.2755 | 71.285586 | 0.00003 | 13,000 |
| | 0 | ∞ | 49.05 | 1.25 | 70.56913 | | |

## RESULTS

To give a first impression on the computed flow field, we show in Figure 2 a visualization of the bubble shape and the velocity field in plane $y = 0.5$ for simulation run M50. The visualization is for time $t = 0.381$ where the vertical coordinate of the bubble center of mass is $x_{com} = 1.5$. Thus, the bubble has risen a vertical distance of four times its equivalent diameter. From the left part of Figure 2 it can be seen that the bubble obeys a closed wake. From the magnified detail in the right part of Figure 2 it becomes evident that the bubble has an oblate ellipsoidal shape.
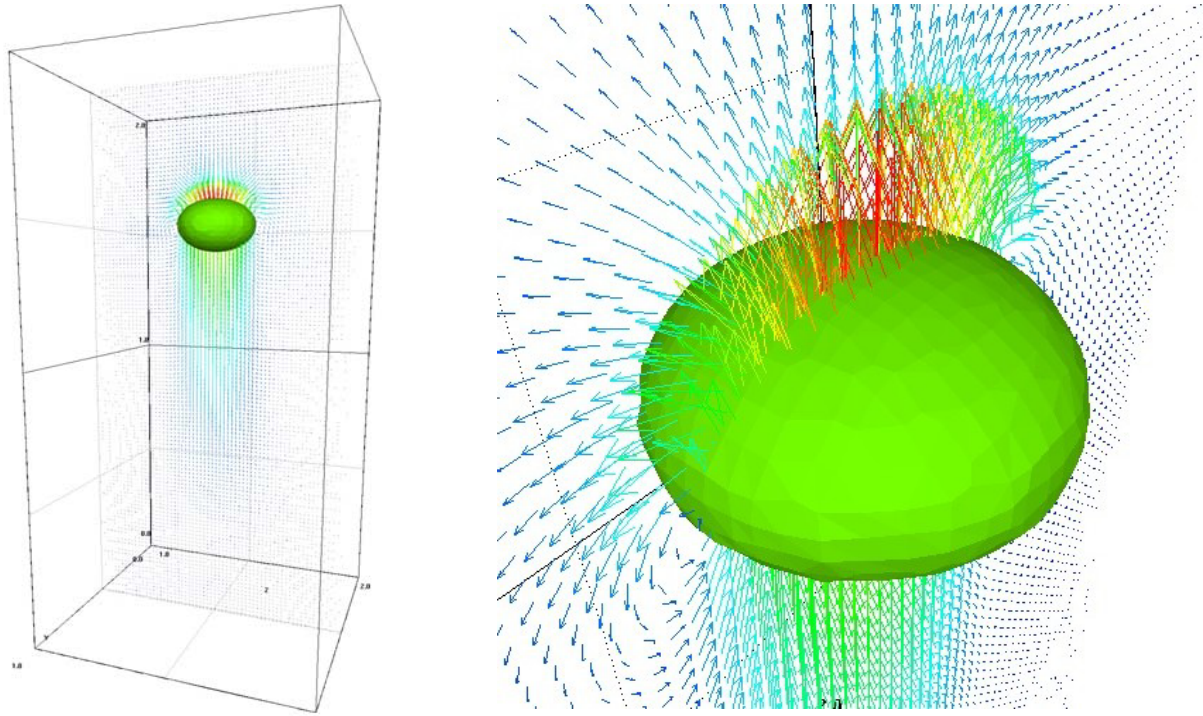
Fig. 2: Instantaneous bubble surface and velocity vectors in plane $y = 0.5$ for run M50

## Bubble rise path

In all the runs the bubbles rise along a vertical rectilinear path. The maximum lateral deviations from this rectilinear path are less than 0.1% of $L_{ref}^*$. In Figure 3 the vertical coordinate of the bubble's center of mass, $x_{com}(t)$, is displayed for the different runs. It is evident that for each density ratio two distinct temporal ranges do exist. In the initial range the bubble's center of mass accelerates and $x_{com}(t) \propto C_1 t^2$. This initial range is followed by a second range where the bubble rises steadily and $x_{com}(t) \propto C_2 t$.
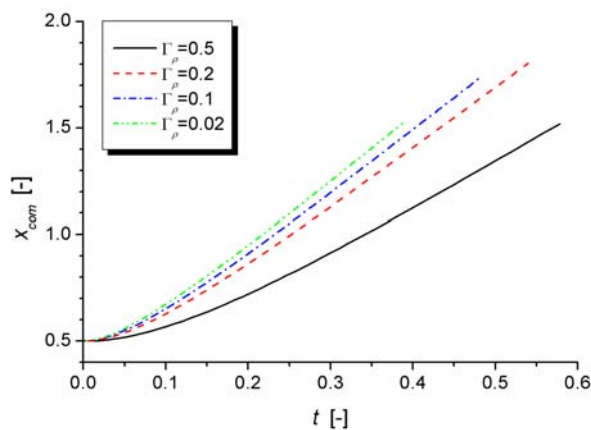


Fig. 3: Computed vertical position $x_{com}(t)$ of bubble centroid for different density ratios.
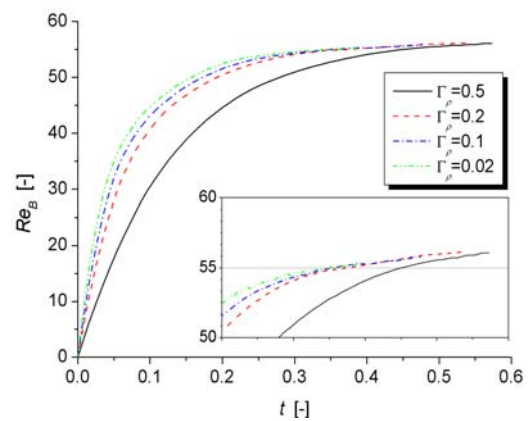
Fig. 4: Temporal evolution of bubble Reynolds number for different density ratios.

Figure 3 shows that the lower $\Gamma_\rho$ the shorter the first range and the higher the coefficient $C_1$. This observation can be explained by a balance between the sum of the unsteady and inertial term and the buoyancy term which is assumed to hold in the first stage of bubble rise. By this and some further assumptions, an ordinary differential equation of second order for

the temporal evolution of the bubble vertical position $x_{com}(t)$ was derived in [18]. Integrating twice and setting the integration constants properly yields

$$x_{com}(t) = 0.5 + \frac{1}{2} \frac{1 - \Gamma_\rho}{C_{AM} + \Gamma_\rho} \frac{g^* L_{ref}^*}{U_{ref}^{*2}} t^2 = 0.5 + C_1(t) \cdot t^2.$$

Here $C_{AM}$ is the added mass coefficient. Using the theoretical value for a spherical bubble, $C_{AM} = 0.5$, it is shown in [18] that the parabola $C_1(\Gamma_\rho) t^2$ is a good fit for the computed data of $x_{com}(t)$ in the initial stage of bubble rise ($t \leq 0.04$) for all values of the density ratio.

## Bubble rise velocity

We now consider the second range in Figure 3, where the dependence of $x_{com}$ on $t$ is linear and thus the bubble rise is steady. Obviously, the bubble rise velocity (the slope in Figure 3) depends on the density ratio: the lower $\Gamma_\rho$ the higher the rise velocity. This result is consistent with the observation of Oka & Ishii [11]. However, the curves displayed in Figure 3 suggest that as $\Gamma_\rho$ approaches zero the slope will be constant and thus the bubble rise velocity becomes independent from $\Gamma_\rho$. Indeed, the last line in Table 1 proves that in the limit $\Gamma_\rho \to 0$ the non-dimensional reference groups entering into the Navier-Stokes equations converge to certain values. Thus, in the limit $\Gamma_\rho \to 0$ the solution will become independent of $\Gamma_\rho$.

We now investigate how the bubble Reynolds number depends on the density ratio. The bubble Reynolds number can be evaluated via relation

$$Re_B = \frac{d_V^*}{L_{ref}^*} \frac{U_B^*}{U_{ref}^*} Re_{ref} = \frac{1}{4} U_B Re_{ref}, \tag{6}$$

where $U_B$ is the (non-dimensional) time derivative of $x_{com}(t)$. The temporal evolution of $Re_B$ for the different runs is displayed in Figure 4. We see that the curves for runs M5, M10, and M50 almost coincide for $t > 0.3$. Also run M2 seems to approach the same value of $Re_B$ which is about 56. In the inset graphic in Figure 4 it can be seen that for all runs $Re_B$ is still slightly increasing and has not yet reached its saturation value. Nevertheless, it was decided not to continue the simulations. Due to the periodic boundary conditions the results might otherwise be no longer representative for the rise of a single bubble but for the rise of a train of periodically released bubbles. Furthermore, due to the interaction of the bubble with the wake of the leading bubble, instabilities may be triggered which may cause a non-rectilinear path. Note that the rectilinear path as well as the value of $Re_B \approx 56$ computed here for a bubble with $E\ddot{o}_B = 3.06$ and $M = 3.09 \cdot 10^{-6}$ agree well with experimental observations for similar values of $(E\ddot{o}_B, M)$ [5].

We now compare the results obtained for the bubble Reynolds number with a semi-empirical correlation. By analogy to two-fluid wave theory, which yields an expression for the phase velocity of inviscid surface tension and gravity waves at a free surface, Mendelson [10] proposed the following formula for the terminal rise velocity of a bubble in the surface-tension or buoyancy force dominated regime

$$U_T^* = \sqrt{\frac{2\sigma^*}{\rho_l^* d_V^*} + \frac{g^* d_V^*}{2}}. \tag{7}$$

While Mendelson noted that the only justification for the above equation is how well it correlates experimental data, Marrucci et al. [9] extended the formula for liquid-liquid systems (i.e. a dispersed liquid drop rising in an immiscible continuous liquid) and proposed

$$U_T^* = \sqrt{\frac{2\sigma^*}{\rho_l^* d_V^*} + \frac{g^* d_V^* \Delta\rho^*}{2\rho_l^*}}. \tag{8}$$

Here, $\Delta\rho^*$ is the difference between the densities of the continuous and dispersed phase. From Eq. (8) it is easy to show that the velocity becomes minimal when the equivalent diameter is

exactly twice the Laplace length, i.e. for $d_V^* = 2\Lambda = 2\sqrt{\sigma^*/(g^*\Delta\rho^*)}$. This condition corresponds to an Eötvös number of $E\ddot{o}_B = 4$.

Recently, Tomiyama et al. [15] gave a physical interpretation why Eq. (8) correlates experimental data so well and noted that multiplying Eq. (8) by $\rho_l^* d_V^*/\mu_l^*$ yields

$$Re_B = \left(2 + \frac{1}{2}E\ddot{o}_B\right)^{0.5}\left(\frac{E\ddot{o}_B}{M}\right)^{0.25}. \tag{9}$$

Thus, $Re_B$ is a function of $E\ddot{o}_B$ and $M$ but does not depend on $\Gamma_\rho$ and $\Gamma_\mu$. For the values $E\ddot{o}_B = 3.06$ and $M = 3.09\cdot10^{-6}$ equation (9) gives $Re_B = 59.3$. Thus, the value $Re_B \approx 56$ obtained in our computational study agrees well with the above theory. Finally, we remark that from equation (9) a rather simple expression for the drag coefficient results [15], which turns out to be a function only of the bubble Eötvös number, namely

$$C_D \equiv \frac{4}{3}\frac{d_V^* g^* \Delta\rho^*}{\rho_l^* U_T^{*2}} = \frac{4}{3}\frac{E\ddot{o}_B}{We_B} = \frac{4}{3}\sqrt{\frac{E\ddot{o}_B^3}{M Re_B^4}} = \frac{8}{3}\frac{E\ddot{o}_B}{E\ddot{o}_B + 4}.$$

## Steady bubble shape

In all the present simulations the steady bubble shape takes the form of an ellipsoid. There is no strict fore-aft symmetry, but the bubble is slightly more flat at its top than at its rear. To quantitatively compare the bubble shape for the runs with different density ratio, we evaluated the three dimensions $a_x$, $a_y$, $a_z$ of the bubble at that instant in time when $x_{com} = 1.5$. We found that in each case the ratio $a_z/a_y$ takes a value between 0.99 and 1. Thus, the bubble is rotationally symmetrical and the lateral walls are obviously sufficiently far away so that they do not affect the bubble shape. The ratios $a_x/a_y$ and $a_x/a_z$ take values between 0.64 and 0.66 in the different runs. With decreasing $\Gamma_\rho$ we observe a small tendency to higher values. This is in agreement with the numerical findings of Ye et al. [20].

Based on experiments for fifty-four dispersed-continuous phase systems Wellek et al. [14] derived empirical relations for the height-to-width ratio ($E$) of non-oscillating bubbles and drops, over a wide range of particle Reynolds numbers. They obtained the relation

$$E = \left(1 + 0.163 E\ddot{o}_B^{0.757}\right)^{-1}, \tag{10}$$

which is valid for $E\ddot{o}_B < 40$ and $M \leq 10^{-6}$. Though the Morton number $M = 3.09\cdot10^{-6}$ used in our numerical study is slightly out of the range for which the latter correlation was derived we note that for $E\ddot{o}_B = 3.06$ correlation (10) yields a value of 0.72. So, with a value of $E \approx 0.66$ the bubble in our computations is distinctively more oblate than relation (10) would suggest. However, relation (10) was obtained for contaminated systems whereas our simulations correspond to a pure system. It is well known [5, p. 182] that bubbles and drops in pure systems are significantly more deformed than corresponding fluid particles in contaminated systems.

## Local velocity profiles

For a reasonable comparison of the local velocity field obtained for the different density ratios we first have to select a representative instant in time. Here, we consider that moment when the vertical position of the bubble centroid is at $x_{com}=1.5$ and thus the bubble has moved four times its initial diameter. As can be seen from Figure 3 this time level differs for the different runs. We compare local velocity profiles along a certain line within our 3D flow domain. In Figure 5 the vertical velocity component $u$ is shown as function of the vertical co-ordinate $x$ for fixed span-wise and wall-normal co-ordinates $y = z = 0.5$. Also shown in Figure 5 is the local profile of the liquid volumetric fraction $f$. In mesh cells filled with liquid the

value of $f$ is 1, in cells filled with gas it is 0, while in cells that instantaneously contain both phases it is $0 < f < 1$. In Figure 5 the profile of $f$ for the different runs almost collapse to a single curve, while the profiles of $u$ are of similar shape, but do not collapse. In Figure 6 we normalize the velocity profiles by the instantaneous bubble rise velocity $U_B$, which differs from run to run. We now find that the normalized velocity profiles collapse to a single curve, too. Thus, when scaled with the bubble rise velocity, the local velocities, both inside the bubble and in the liquid are identical and are invariant with respect to a variation of the density ratio.
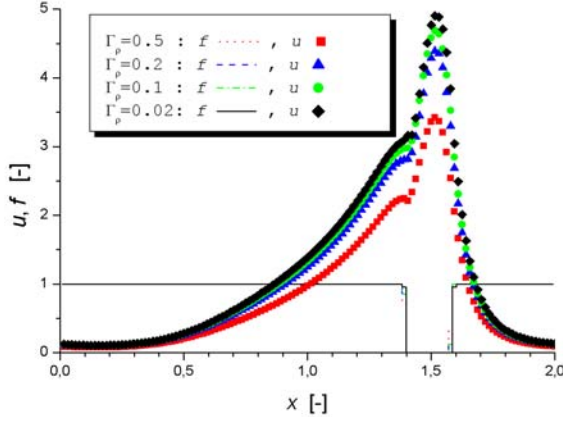


Fig. 5: Vertical profile of local instantaneous vertical velocity, $u$, and liquid volume fraction, $f$, for $y=z=0.5$.
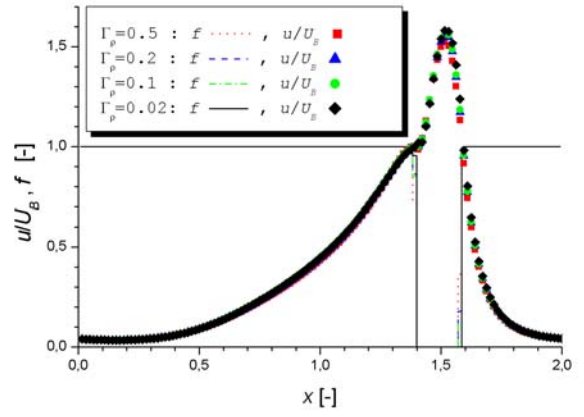
Fig. 6: Vertical profile of normalized local instantaneous vertical velocity $u/U_B$ and liquid volume fraction, $f$, for $y=z=0.5$.

## CONCLUSIONS

A numerical study is presented in which the influence of the gas-liquid density ratio ($\Gamma_\rho$) on bubble shape, Reynolds number ($Re_B$) and local velocity field is investigated. For fixed values of the Morton number ($M = 3.09 \cdot 10^{-6}$) and the bubble Eötvös number ($E\ddot{o}_B = 3.06$) and for a unity viscosity ratio we performed 3D volume-of-fluid computations for four different cases, where the liquid density is 2, 5, 10, and 50 times the gas density. All the simulations result in an oblate ellipsoidal bubble that rises steadily along a rectilinear path. The results indicate that due to the added mass force the density ratio has a notable influence on how fast the bubble accelerates from rest to its terminal velocity. Once the bubble reached its terminal velocity, however, the functional dependence of both, the bubble Reynolds number and the bubble's height-to-width ratio on the density ratio appears to be very weak. For all the four cases the value of $Re_B$ is about 56. This value agrees well with a relation derived by two-phase wave theory. In this relation $Re_B$ depends on $E\ddot{o}_B$ and $M$ but does not depend on $\Gamma_\rho$ and $\Gamma_\mu$. For the values of $E\ddot{o}_B$ and $M$ considered here this relation yields $Re_B = 59.3$.

By the results obtained we conclude that for an ellipsoidal bubble rising steadily on a rectilinear path the bubble shape and non-dimensional terminal rise velocity, expressed by the bubble Reynolds number, are not notably affected by the gas-to-liquid density ratio as long as there is similarity of $E\ddot{o}_B$, $M$ and $\Gamma_\mu$. At present this result is demonstrated only for the specific parameters of $E\ddot{o}_B$, $M$, and $\Gamma_\mu$ given above. However, the good agreement with two-phase wave theory indicates that a similar conclusion may also hold for other values of $E\ddot{o}_B$ and $M$ as long as the bubble is in the surface tension or buoyancy dominated regime (as opposed to the viscous regime) and rises steadily on a rectilinear path. For this kind of bubbles then rather universal relations for bubble Reynolds number and drag coefficient in terms of $E\ddot{o}$ and $M$ should exist. So, the correlations for the drag coefficient given in [15] which were verified

by experiments where $\Gamma_\rho \approx 0.001$ may in fact be applicable to gas-liquid or liquid-liquid systems of any density ratio.

We showed that similarity holds not only for bubble shape and steady bubble Reynolds number, but also for the exterior flow field, induced by the bubble motion within the liquid phase. This might suggest that rather universal models for the turbulence induced by bubbles rising almost steadily in dilute gas-liquid flows may be derived in terms of $E\ddot{o}_B$ and $M$. Furthermore, we conclude that for steady bubbles it is possible to perform computationally efficient direct simulations with density ratio of order 0.1 while the results are of relevance for gas-liquid systems with density ratio of order 0.001.

The present findings are not directly verified by experiments yet. To verify them it would be necessary to perform experiments with at least two sets of different gas-liquid or liquid-liquid systems which obey the same Morton number but a significantly different density ratio. If the Morton number of both systems is the same, then similarity in the Eötvös number can easily be ensured by properly setting the bubble diameters. It may be more difficult to ensure similarity of the viscosity ratio of the different gas-liquid or liquid-liquid systems. However, there is experimental evidence that for a fixed Morton number the influence of the viscosity ratio on the bubble Reynolds number is small: Clift et al. [5, p. 173] compare experimental results obtained by different workers for $Re_B$ as a function of $E\ddot{o}_B$ for systems with essentially the same Morton number ($M \approx 2 \cdot 10^{-10}$) but widely different values of $\Gamma_\mu$ (0.35 to 20). Though the data exhibit some scatter, it is evident that $Re_B$ does not vary systematically with $\Gamma_\mu$.

# REFERENCES

[1]     Brackbill, J.U., Kothe, D.B., Zemach, C.: A Continuum Method for Modelling Surface Tension. J. Comput. Phys. 100 (1992) 335-354.

[2]     Bunner, B., Tryggvason, G.: Dynamics of homogeneous bubbly flows. Part I: Motion of the bubbles. Submitted to Journal of Fluid Mechanics.

[3]     Chen, L., Garimella, S.V., Reizes, J.A., Leonardi, E.: The development of a bubble rising in a viscous liquid. J. Fluid Mech. 387 (1999) 61-96.

[4]     Churchill, S.W.: A Theoretical Structure and Correlating Equation for the Motion of Single Bubbles. Chem. Eng. Process. 26 (1989) 269-279.

[5]     Clift, R., Grace, J.R., Weber, M.E.: Bubbles, Drops, and Particles. Academic Press, 1978.

[6]     Dandy, D.S., Leal, L.G.: Buoyancy-driven motion of a deformable drop through a quiescent liquid at intermediate Reynolds number. J. Fluid Mech. 208 (1989) 161-192.

[7]     Grace J.R.: Shapes and velocities of bubbles rising in infinite liquids. Trans. Instn. Chem. Eng. 51 (1973) 116-120.

[8]     Juncu, Gh.: A numerical study of steady viscous flow past a fluid sphere. Int. J. Heat Fluid Flow 20 (1999) 414-421.

[9]     Marrucci, G., Apuzzo, G., Astarita, G.: Motion of Liquid Drops in Non-Newtonian Systems. AIChE Journal 16 (1970) 538-541.

[10]    Mendelson, H.D.: The prediction of Bubble Terminal Velocities from Wave Theory. AIChE Journal 13 (1967) 250-253.

[11]    Oka, H., Ishii, K.: Numerical analysis on the motion of gas bubbles using level set method. J. Physical Soc. Japan 68 (1999) 823-832.

[12]    Sabisch, W.: Dreidimensionale numerische Simulation der Dynamik von aufsteigenden Einzelblasen und Blasenschwärmen mit einer Volume-of-Fluid Methode. Forschungszentrum Karlsruhe, Wissenschaftliche Berichte FZKA 6478, June 2000 (http://hikwww4.fzk.de/hbk/literatur/FZKA_Berichte/FZKA6478.pdf).

[13]    Sabisch, W., Wörner, M., Grötzbach, G., Cacuci, D.G.: 3D volume-of-fluid simulation of a wobbling bubble in a gas-liquid system of low Morton number. Proc. 4th Int. Conf.

on Multiphase Flow (ICMF), New Orleans, LA, U.S.A., May 27 - June 1, 2001, CD-ROM, paper 244.

[14] Sussman, M., Puckett, E.G.: A Coupled Level Set and Volume-of-Fluid Method for Computing 3D and Axisymmetric Incompressible Two-Phase Flows. J. Comput. Phys. 162 (2000) 301-337.

[15] Tomiyama, A., Kataoka, I., Zun, I., Sakaguchi, T.: Drag Coefficients of Single Bubbles under Normal and Micro Gravity Conditions. JSME International Journal Series B 41 (1998) 472-479.

[16] Tryggvason, G., Bunner, B., Ebrat, O., Tauber, W.: Computations of multiphase flows by a finite difference/front tracking method. I. Multifluid flows. Von Karman lecture notes , the von Karman Institute (1998).

[17] Wellek, R.M., Agrawal, A.K., Skelland, A.H.P.: Shape of liquid drops moving in liquid media. AIChE Journal 12 (1966) 854-862.

[18] Wörner, M.: The influence of gas-liquid density ratio on shape and rise velocity of an ellipsoidal bubble: a numerical study by 3D volume-of-fluid computations. Proc. 1st Berlin Workshop on Transport Phenomena with moving Boundaries, October 11-12, 2001, Berlin, Germany.

[19] Wörner, M., Sabisch, W., Grötzbach, G., Cacuci, D.G.: Volume-averaged conservation equations for volume-of-fluid interface tracking. Proc. 4th Int. Conf. on Multiphase Flow (ICMF), New Orleans, LA, U.S.A., May 27 - June 1, 2001, CD-ROM, paper 245.

[20] Ye, T., Shyy, W., Chung, J.N.: A fixed-grid, sharp-interface method for bubble dynamics and phase change. J. Comput. Phys. 174 (2001) 781-815.